IEEE Access
Multidisciplinary | Rapid Review | Open Access Journal

Received December 16, 2019, accepted December 26, 2019, date of publication January 1, 2020, date of current version January 8, 2020.

Digital Object Identifier 10.1109/ACCESS.2019.2963444

An Intuitionistic Kernel-Based Fuzzy C-Means Clustering Algorithm With Local Information for Power Equipment Image Segmentation

FANKUI HU, HAIBING CHEN, AND XIAOFEI WANG
College of Electrics Engineering, Heilongjiang University, Harbin 150080, China
Corresponding author: Xiaofei Wang (nk_wxf@hlju.edu.cn)

This work was supported in part by the National Natural Science Foundations of China under Grant 61871150, and in part by the National Key Research and Development Program of China under Grant 2016YFB0502502.

ABSTRACT With the transformation of the national energy and power sector, the steady advancement of intelligent power grid construction and the continuous improvement of the Ubiquitous Power Internet of Things technology framework, it has further requirements for realizing state comprehensive awareness and efficient processing of information data, and has been widely used in power equipment. The infrared image recognition technology, which has been widely used in thermal fault diagnosis of power equipment, also requires deeper research. For traditional Intuitionistic Fuzzy C-means (IFCM) algorithm for image segmentation is sensitive to the clustering center lead to low final clustering precision and detail, the time complexity and the high shortage. The paper puts forward a kind of applicable to power equipment of the infrared image segmentation based on space distribution information of Intuitionistic Fuzzy clustering algorithm. Non-target objects with high intensity and uneven image intensity in infrared image have strong interference to image segmentation. The proposed algorithm can effectively suppress the interference. Firstly, the gaussian model is introduced into the global spatial distribution information of power equipment to improve the IFCM. Secondly, the spatial operator optimization membership function of local spatial information is used to solve the problem of edge blurring and uneven image intensity. Through experiments on the data set containing 300 infrared images of power equipment, the relative regional error rate is about 10%, which is less affected by the change of fuzzy factor m. The effectiveness and applicability of this algorithm are verified, which is obviously better than other comparison algorithms.

INDEX TERMS Intuitionistic fuzzy clustering, infrared image, Gaussian model, local information.

I. INTRODUCTION

The emergence and rapid development of remote sensing of UAVs (Unmanned Aerial Vehicle) has enabled remote sensing scientific research to move from macro to micro. Local overheating phenomenon caused by power facility failure, the use of thermal infrared imagers to find thermal faults and then manual diagnosis is the main diagnostic tool widely used in the field of power grids. UAV remote sensing has the characteristics of high resolution and flexibility, and it can efficiently and accurately explore ground information. Therefore, infrared drone technology is one of the development directions of real-time fault diagnosis of power equipment in the future, providing technology protection for national security and interests.

Based on the imaging principle of the temperature characteristics of the object, the imaging environment of infrared image is not limited by weather or lighting conditions, and infrared images have a wide range of applications in military and civilian applications. With the introduction and continuous development of the concept of smart grid in recent years, infrared imaging technology has played an indispensable role in the field of power grid fault diagnosis [1], temperature monitoring [2], etc., which makes the application of infrared imaging technology have important civilian significance. Since the contrast of structure and shape information in the infrared image of power equipment is not high, infrared segmentation is a key step in target recognition and analysis.

The associate editor coordinating the review of this manuscript and approving it for publication was Md. Asikuzzaman.

In general, the result will play a key role in improving the accuracy of the recognition process. However, due to the limitations of the infrared image itself, it is difficult to get accurate true gray value distinguishes the result. Uneven heat dissipation on the surface of power equipment results in uneven intensity distribution of the target, low image resolution due to edge blur, and loss of texture detail is also a common phenomenon in processing infrared images. In addition, the substation as a complex environment covers issues such as fog and rain, surface reflections of equipment and high-intensity effects of non-electric equipment. For these reasons, the segmentation of infrared power equipment is still a challenging task. Conventional threshold-based methods can be applied to infrared power device segmentation, including the Otsu and the minimum error threshold for simple and efficient segmentation of dark targets in infrared images. However, when the image contains a complex multimodal structure, the performance of these traditional segmentation methods will be significantly reduced. An adaptive local double threshold segmentation method proposed for infrared images of different histograms takes a long time and may generate a large number of negative correlation regions. In addition, non-target objects, edge blur and intensity non-uniformity presented in infrared images, etc. will have different degrees of impact on the above methods.

In recent years, various methods have been proposed for infrared image segmentation of power equipment. The PCNN segmentation improvement algorithm is proposed [3]. The PCNN algorithm is combined with the intra-class absolute difference method, through the optimization of parameters and thresholds, the infrared image of power equipment is segmented, and the edge detail features are well preserved. A segmentation method based on Otsu algorithm and region growing algorithm is proposed [4]. It eliminates background interference and accurately extracts the target area. Another method is to use the bat algorithm to improve the spatial information entropy, and quickly search for the optimal segmentation threshold, and improving the segmentation effect and efficiency through the threshold segmentation experiment [5]. Power equipment is segmented by Niblack which using particle swarm optimization [6]. Extracting the target area from the device image by automatically searching for the optimal segmentation threshold of non-overlapping rectangular neighborhoods in the Niblack. The clustering algorithm can also be used for infrared segmentation of power equipment. The k-means clustering algorithm is a classical clustering method with low computational complexity and fast convergence [**?**]. However, its relative sensitivity to noise means that the distance between different categories in the image is required to be relatively distant, which is not common in infrared images.

In recent years, fuzzy c-means clustering algorithm (FCM) and its corresponding improved algorithm have been widely used in image segmentation and other fields. The traditional FCM algorithm lacks spatial information and is less robust to noise, which makes the segmentation effect based on FCM algorithm less than ideal. Therefore, a lot of work needs to be done on the introduction of spatial information. This type of method combines local information with the intensity information of the image to overcome the lack of noise and non-uniformity, achieves certain results. However, these improvements limit spatial information to local areas, which means that the effect of high-intensity non-target objects on image segmentation still exists. Aiming at the uncertainty of the target edge and the non-uniformity of the intensity distribution in the infrared image, an algorithm is proposed, which uses Atanassov's intuitionistic fuzzy set theory to study the membership degree, non-affiliation and Hesitation and other factors [8]. The visual fuzzification of data clustering is further proposed [9], where data point x_p is represented as $(\lambda_p, \mu_p, \nu_p)$ instead of a single m λ_p.

Xu, Wu, and others combine intuitionistic fuzzy set theory with fuzzy set theory [10], they replaced the fuzzy distance in objective function with the intuitionistic fuzzy distance. The degree of hesitation in existence provides a good method for dealing with the uncertainty of data points. The intuitionistic fuzzy set theory and the kernel-based fuzzy c-means are combined to select parameters by evolutionary algorithms [11]. The evolutionary kernel intuitionistic fuzzy c-means clustering algorithm (EKIFCM) performs more stable under noise interference conditions and improves the accuracy rate. A new probability similarity measurement method and clustering technique are also proposed to design adaptive weights for intuitionistic fuzzy distances [12]. However, image segmentation is a special classification that targets images and involves more spatial and semantic information. In [13], the intuitionistic fuzzy set and rough set are combined with the statistical feature extraction technology. The intuitionistic fuzzy set is used to extract the regions of interest, and the gray scale co-occurrence matrix is used for feature extraction. In [14], an adaptive interval 2-type intuitionistic fuzzy c-means clustering algorithm (A-PSO-IT2IFCM) based on alternating particle swarm optimization was proposed to obtain the appropriate cluster center initialization and was applied to color image segmentation. In recent years, the IFCM algorithm pays more attention to the feature point clustering problem, which determines that the segmentation effect may not be ideal when the image has strong spatial correlation. To this end, for the intensity non-uniformity and non-high-intensity targets existing in the infrared image of the substation equipment, an intuitionistic fuzzy clustering method based on local information is proposed.

The main work of this paper includes: 1) Proposing a fuzzy clustering algorithm combined with global distribution information, which is used to segment the target of high-intensity non-power equipment existing in the image. In the clustering process, the Gaussian kernel function is used to calculate the spatial distance from the target point to the target centroid. 2)Introducing the local spatial distribution information into the IFCM to detect the distance, so as to ensure the balance between image details and inhibiting the uneven intensity of the image. 3) Calculating the neighborhood membership of

the objective function by the Lagrange Multiplier method and comparing it with the traditional IFCM segmentation method.

II. INTUITIONISTIC FUZZY CLUSTERING ALGORITHM (IFCM)

A. FUZZY C-MEANS CLUSTERING ALGORITHM

Fuzzy set theory was first proposed by Zadeh in 1965 [15]. After years of development, some improved fuzzy sets are gradually proposed, such as type 2 fuzzy sets [16], interval type 2 fuzzy sets [17], intuitionistic fuzzy sets [8], etc. These extended fuzzy sets can deal with more uncertainties and have been widely applied. The fuzzy c-means algorithm was proposed by Dunn in 1973 [18], and then promoted by Bezdek J.C. [19]. The algorithm minimizes the objective function J by iteratively updating membership and cluster centers. The objective function of the FCM algorithm is defined as follows:

$$J_m(U, X) = \sum_{j=1}^{c} \sum_{k=1}^{n} u_{jk}^m d^2(x_k, v_j) \tag{1}$$

To meet the following restrictions:

$$\sum_{j=1}^{c} u_{jk} = 1, u_{jk} \in [0, 1] \tag{2}$$

where U is the fuzzy membership matrix of the pixel, the number of rows is equal to the number of cluster centers c, and the number of columns is equal to the number of pixels of the image n, x_k is the kth data point, v_j is the j-class clustering prototype, u_{jk} is the fuzzy membership of the kth cluster sample to the jth cluster center, $m \in [0, \infty]$ as a fuzzy weighted index changes the membership of x_k. As distortion, $d^2(x_k, v_j)$ is generally expressed as Euclidean distance:

$$d^2(x_k, v_j) = \| x_k - v_j \|^2 \tag{3}$$

Since the clustering effect of the image is best when the objective function obtains the minimum value, the minimum roots of can be obtained after iterative calculation according to the Lagrange Multiplier Method:

$$u_{jk} = [\sum_{i=1}^{c} \frac{\|x_k - v_k\|}{\|x_k - v_i\|}]^{-\frac{2}{m-1}} \tag{4}$$

$$v_j = \frac{\sum_{k=1}^{n} u_{jk}^m x_k}{\sum_{k=1}^{n} u_{jk}^m} \tag{5}$$

B. INTUITIONISTIC FUZZY C-MEANS ALGORITHM (IFCM)

The core theory of the FCM algorithm described in Section 2.1 is to extend the eigenfunction (which can only take 0 or 1) to a membership function of any value in the interval [a, b]. However, the membership function as a single function does not indicate the uncertainty of the existence of things. That is to say, the FCM algorithm cannot accurately describe the existence of the situation except affirmation and negation, therefore this limitation led to the birth of the intuitionistic fuzzy c-means (IFCM) algorithm [8]. The theory of intuitionistic fuzzy sets proposes the concept of hesitation, which expresses the state with neutral attributes, and more completely and accurately depicts the fuzzy information existing in objective reality. The n-dimensional data set X can be represented by IFS as follows:

$$A = \{(x, u_A(x), v_A(x)), x \in X\} \tag{6}$$

where $u_A(x)$ and $v_A(x)$ respectively represent the membership and non-membership functions of element x.

$$u_A(x) : X \to [0, 1]; v_A(x) : X \to [0, 1] \tag{7}$$

The formulas respectively indicate the extent to which element x in X absolutely belongs to subset A of X and absolutely does not belong to subset A. In Atanassov's intuitionistic fuzzy set theory [20], the sum of membership and non-membership should satisfy $0 \le u_A(x) + v_A(x) \le 1$. Therefore, the above degree of hesitation is produced, and its effect is defined as follows:

$$\pi_A(x) = 1 - u_A(x) - v_A(x) \tag{8}$$

Set an image to I, x is an image pixel, and its gray value ranges from 0 to 1. According to the intuitionistic fuzzy data theory of Vlachos and Sergiadis [21], the membership degree is defined as the normalized gray value of the image:

$$u_A(x) = \frac{x - I_{min}}{I_{max} - I_{min}} \tag{9}$$

where I_{max} and I_{min} respectively represent the maximum gray value and the minimum gray value of image I. Sugeno [22] used the negative function to calculate the non-affiliation of the intuitionistic fuzzy set as follows:

$$v_A(x) = \frac{1 - u_A(x)}{1 + \lambda u_A(x)} \tag{10}$$

where λ is a normal number, which guarantees that the sum of membership and non-affiliation will not be greater than 1.

Further, assume that d: $IFS(X) \times IFS(X) \to [0, 1]$. If d is the distance measure between intuitionistic fuzzy sets (IFSs) [23], the following attributes should be satisfied:

1) $0 \le d(A, B) \le 1$
2) $d(A, B) = 0$ If and only if $A = B$
3) $d(A, B) = d(B, A)$
4)If $A \subseteq B \subseteq C$ $(A, B, C \in IFSs(X))$, then $d(A, B) \le d(A, C)$ and $d(B, C) \le d(A, C)$ The normalized Euclidean distance between A and B in IFSs is defined as follows:

$$d_{IFS}(A, B) = \frac{1}{2n} \sum_{i=1}^{n} \{(u_A(X_i) - u_B(X_i))^2 + [v_A(X_i) - v_B(X_i)]^2 + [\pi_A(X_i) - \pi_B(X_i)]^2\} \tag{11}$$

Furthermore, an improved normalized Euclidean distance is proposed [24], defined as follows:

$$d(A_1, A_2) = \frac{1}{2n}\sum_{i=1}^{n}\{p_{12}(u_{A1}(X_i) - u_{A2}(X_i)]^2 + q_{12}[v_{A1}(X_i) - v_{A2}(X_i)]^2 + \rho(A_1, A_2)(\pi_{A1}(X_i) - \pi_{A2}(X_i))^2\} \quad (12)$$

where p_{12},q_{12} and $\rho(A_1, A_2)$ can be used as adaptive weights based on actual data [25]. Define the objective function of IFCM as follows:

$$J_{IFCM} = \sum_{j=1}^{c}\sum_{k=1}^{n} u_{jk}^m d_{IFS}^2(x_k, v_j) \quad (13)$$

where d_{IFS}^2 defined above is the Euclidean intuitionistic fuzzy distance. Based on this, the iterative formula of membership degree and cluster centroid based on Lagrange Multiplier method is given as follows:

$$u_{jk} = [\sum_{i=1}^{c}\frac{d_{IFS}(x_k, v_j)}{d_{IFS}(x_k, v_i)}]^{\frac{2}{m-1}} \quad (14)$$

$$u_A(v_j) = \frac{\sum_{k=1}^{n} u_{jk}^m u_A(x_k)}{\sum_{k=1}^{n} u_{jk}^m} \quad (15)$$

$$v_A(v_j) = \frac{\sum_{k=1}^{n} u_{jk}^m v_A(x_k)}{\sum_{k=1}^{n} u_{jk}^m} \quad (16)$$

$$\pi_A(v_j) = \frac{\sum_{k=1}^{n} u_{jk}^m \pi_A(x_k)}{\sum_{k=1}^{n} u_{jk}^m} \quad (17)$$

In the IFCM algorithm, the cluster center v_j is expressed as $v_j = u_A(v(j) \bigcup v_A(v_j) \bigcup \pi_A(v_j)$. The solution of the objective function can be obtained by iterative equations (14)-(17), and the convergence of the IFCM algorithm is proved by equations (11)-(14) [26], wherein the above solution is a local minimum value of the objective function defined in equation (13).

III. POWER EQUIPMENT IMAGE SEGMENTATION

Usually, in actual operation, the power equipment is not the only highlighted area in the infrared image [27]. For example, artificial buildings and commuter vehicles in the substation have higher temperatures, so these objects exhibit gray values intensity similar to those of the power equipment in the infrared image, which affects the identification of electrical equipment. In addition, the intensity distribution of the infrared image is uneven and the edges are blurred, which makes the segmentation of the infrared image more difficult [28]. Aiming at the defects and deficiencies of the existing infrared image segmentation methods for power equipment, this paper proposes several improvement measures [29]. It mainly includes: 1) introducing global distribution information in the form of Gaussian model; 2) introducing IFCM into image segmentation based on local intensity distribution information.

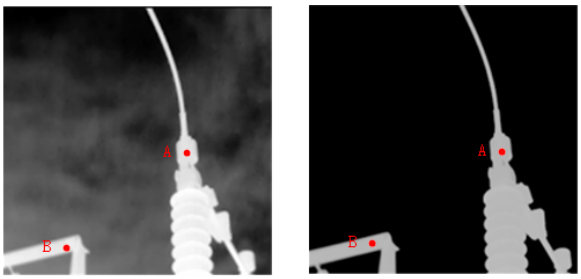

FIGURE 1. (a) Original grayscale image (b) FCM processing imageOriginal image and FCM segmentation result.

A. IMPROVEMENT OF GLOBAL DISTRIBUTION INFORMATION BASED ON GAUSSIAN MODEL

Traditional FCM methods often divide pixels with relative intensity relative to the target into target classes. Due to the lack of global spatial information, noise, high gray value intensity objects and other interference have a greater impact on the segmentation results. In equation (1), for $\forall x$, the membership degree u_{jk} satisfies $\sum_{k=1}^{n} u_{jk} = 1$, which can be regarded as a weight coefficient. If $m = 1$, the FCM is converted to a hard c-means cluster with a membership value of 0 or 1. Further, if $m \geq 1$, in order to minimize the objective function, for each x, its larger weight will tend to be assigned to the smaller $\|x_k - v_j\|^2$ $(j = 1, \ldots, c)$. However, the distance metric $\|x_k - v_j\|^2$ only points to the intensity of the pixel gray value, which also causes an error in the image classification, because under this metric, the pixels of the power device are indistinguishable from other pixels having similar gray values [30]. As shown in Fig. 1, points A and B are improperly divided into the same class by the FCM algorithm.

In response to the above problem, the global distribution information is introduced into the objective function of the FCM. The possible areas of the power device in the image can be approximated by a variety of methods, in fact, only an approximate position is required [31], which includes a larger area of the power device than the power device in the image. Therefore, considering the time cost and positioning effect, this paper adopts the positioning method.

A basic assumption is that the probability of a pixel becoming a target increases as the distance from the possible area of the power device to the centroid becomes shorter [32]. Therefore, the possibility that it belongs to the background is reduced. The fluctuations in fuzzy clustering should be reflected in the membership degree. Therefore, in order to adapt to the position change, the following coefficient W_{jk} is designed to be substituted into the objective function J to

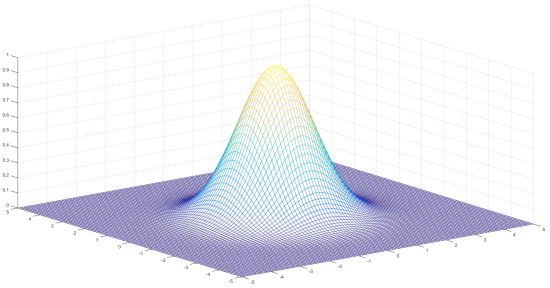

FIGURE 2. Two-dimensional gaussian distribution surface diagram.

enhance the membership degree:

$$J = \sum_{j=1}^{c} \sum_{k=1}^{n} W_{jk} u_{jk}^{m} \|x_k - v_j\|^2 \tag{18}$$

$$W_{jk} = [\frac{\beta}{\frac{1}{\sqrt{2\pi}} \exp(-\frac{\alpha \|pos(k) - pos(c)\|^2}{2\sigma^2})}] \tag{19}$$

$$\Phi_{jk} = \begin{cases} -\exp[e^{\gamma(\sqrt{\|pos(k)-pos(c)\|^2} - \frac{diag}{2})} - 1] & \text{j=1} \\ \exp[e^{\gamma(\sqrt{\|pos(k)-pos(c)\|^2} - \frac{diag}{2})} - 1] & \text{j=2} \end{cases} \tag{20}$$

where $pos(k)$ is the coordinate of pixel k and $pos(c)$ is the coordinate of the centroid of the possible area of the power equipment. α and β are constants, respectively $0.75 \times 10_{-3}$ and 0.2. σ is the variance of the Gaussian model, which is generally 3. The symbol *diag* refers to the diagonal of the possible area found in this article. γ is a parameter that controls the range of distance to the target center. The denominator of W_{jk} uses a Gaussian model, indicating that the closer the pixel is to the centroid, the more likely it is to belong to the target [33]. When the pixel is at the centroid position, the probability intensity curve peaks, as shown in Figure 2.

W_{jk} participates in the iterative process as part of the distance metric. When the denominator of W_{jk} is represented by a Gaussian model, the surface of the expression is basin-shaped. A minimum point will appear at the target centroid position. Let the background belong to the first category, and the power equipment belongs to the second category. For class 2, since the denominator of W_{jk} obeys the Gaussian distribution, the distance metric from the far center of the centroid is large. Conversely, for class 1, the distance metric away from the centroid point will be small because the index Φ_{1k} is negative [34]. Therefore, the membership of the power equipment will be very high. As shown in equation (20), it is different in the case of reflecting the target and the background.

The image centroid is the center of gravity of the image grayscale, so can be calculated by the gray center of gravity method [35]. As a kind of weighted centroid method with gray squared weight, the gray center of gravity method treats the gray value of each pixel in the region as the "quality" of the point, which can represent the centroid coordinate (x_0, y_0)

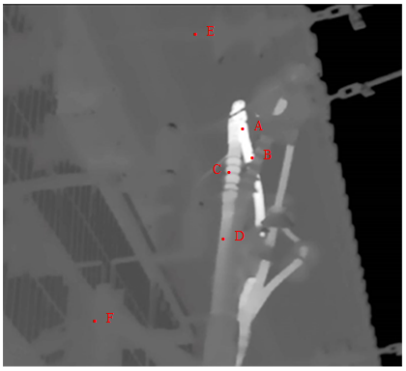

(a) The original image, point A – F sorted by distance

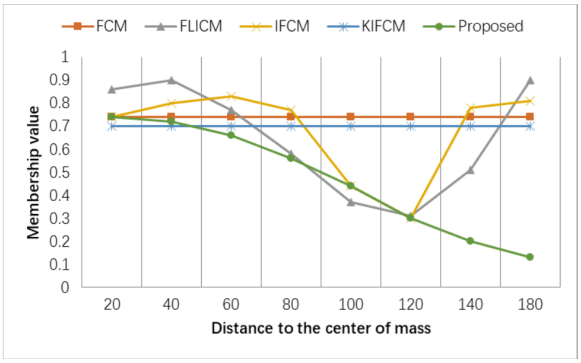

(b) The membership degree of the second class was obtained by different clustering method

FIGURE 3. Membership value of power equipment at different positions under the same intensity.

of the power equipment target S as follows:

$$\begin{cases} x_0 = \dfrac{m_{10}}{m_{01}} = \dfrac{\sum\limits_{(u,v)\in S} uP(u,v)}{\sum\limits_{(u,v)\in S} P(u,v)} \\ y_0 = \dfrac{m_{01}}{m_{00}} = \dfrac{\sum\limits_{(a,b)\in S} vP(u,v)}{\sum\limits_{(a,b)\in S} P(u,v)} \end{cases} \tag{21}$$

where $P(a, b)$ is the weight, the gray center of gravity method extracts the energy center in the region, and has a better positioning effect when the device target S and the background have larger gray difference values.

Theorem 1: For l and p with the same pixel, if $\|pos(l) - pos(c)\|^2 > \|pos(p) - pos(c)\|^2$, there will be $W_{jl}\|x_l - v_j\|^2 < W_{jp}\|x_p - v_j\|^2$ for class 1 (can be proved by d_{lc}^2 and d_{pc}^2 respectively). Similarly, this article can also be obtained under the same conditions for class 2 with $W_{jl}\|x_l - v_j\|^2 > W_{jp}\|x_p - v_j\|^2$. According to the above properties, it can be inferred that the distance between the pixels of the same intensity and the center of the first type of cluster will decrease as the spatial distance from the target centroid increases [36].

Figure 3 above shows the membership values of A-F points to Class 2 obtained by different clustering methods. Select the point A-F of the same intensity from Figure 3(a),

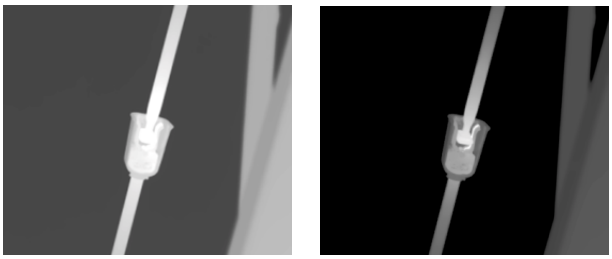

(a) Original image (b) FCM processing imag

(c) The improved result diagram

FIGURE 4. Segmentation result diagram.

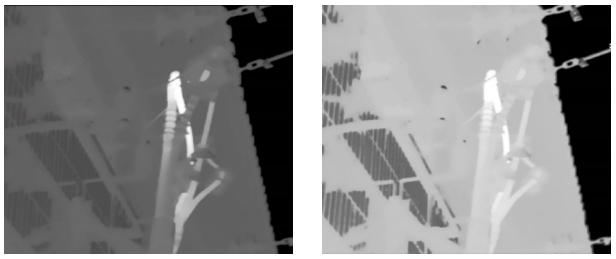

(a) Original image (b) FCM processing image

(c) Improved result diagram using W_{jk} and $\Phi_{jk} = \pm 1$ (d) Improved result diagram using Φ_{jk} in Eq.17

FIGURE 5. Results of different algorithms.

where A is the closest point to the power equipment and F is the point farthest from the power equipment. According to the real background information in the image, only points A and B belong to the power equipment, and others are the background of the non-power equipment [37]. The red and green curves are the membership values obtained by FCM and KIFCM. It can be seen from this paper that due to the lack of spatial information, the membership values calculated by points at different locations are the same. In the case of low contrast, regardless of the classification of spatial information will result in a higher error rate. The yellow and purple curves are the membership values obtained by FLICM and IFCM. It is obviously affected by local spatial information, so points at different locations have different membership values. Similarly, in the case of low contrast, the function of local information is still limited [38]. The main reason is that the homogeneity of local regions may have a negative impact on clustering, resulting in the same misclassified state throughout the region. The blue curve is the result of adding global space information. Compared with other curves, as $W_{2k}\|x_k - v_2\|^2$ increases, the degree of membership will gradually decrease with increasing distance centroid. As the distance increases, the degree of membership decreases, and a higher accuracy rate is obtained [39], thus demonstrating the effectiveness of introducing global distribution information.

Theorem 2: When the distance to the centroid d_{kc} exceeds the radius of the possible region $diag/2$, the gain of the index Φ_{jk} will increase relatively.

In the above theorem, Φ_{jk} plays an important role. The ever-increasing exponential function guarantees that certain noise or high gray-scale intensity objects will not be misclassified. As shown in Figure 4, in some cases, weather factors such as haze may have a certain negative impact on segmentation. Because FCM cant recognize clouds and electrical equipment well, the results will be clearly unsatisfactory. In this case, W_{jk} and the fixed value Φ_{jk} can effectively solve the problem. This is because the gray value of the sky pixel is near the midpoint of the two cluster centers. Regardless of the value of the pixel, W_{jk} is easy to record it into a class. However, there are some bright areas in the image that do not contain device targets. If only the intensity is considered, the pixels in these areas are usually closer to the cluster centroid of the power equipment class.

In fact, the range of W_{jk} has a limited range, which affects the processing and avoids misclassification. When the index is fixed to 1 and - 1 in this paper, the segmentation result is shown in Figure 5 (b). Compared with the FCM calculation results, the cloud area is reduced, but some clouds are still divided into power equipment. This indicates that the gray value intensity is still the main factor determining the pixel class. When Φ_{jk} increases as the distance from the centroid increases, W_{jk} will increase by several orders of magnitude. When the distance is far enough, the influence of spatial information is greater [40]. In this case, even if the pixel has high intensity, it will not be classified into a power device class, as shown in FIG. 5(d).

B. IMPROVED IFCM ALGORITHM BASED ON LOCAL INTENSITY DISTRIBUTION INFORMATION

The Intuitionistic Fuzzy Set (AIFS) theory proposed by Atanassov is used as an extension of fuzzy set theory. It extends the concept of affiliation to affiliation and non-affiliation, and satisfies $0 \leq u_A(x) + v_A(x) \leq 1$, and obtains hesitation through the formula $\pi_A(x) = 1 - u_A(x) - v_A(x)$. AIFS is a simulation of the hum Due to the principle of

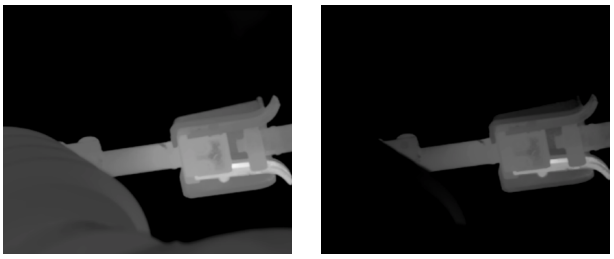

(a) Original image (b) FCM segmentation result diagram

FIGURE 6. Segmentation of uneven image.

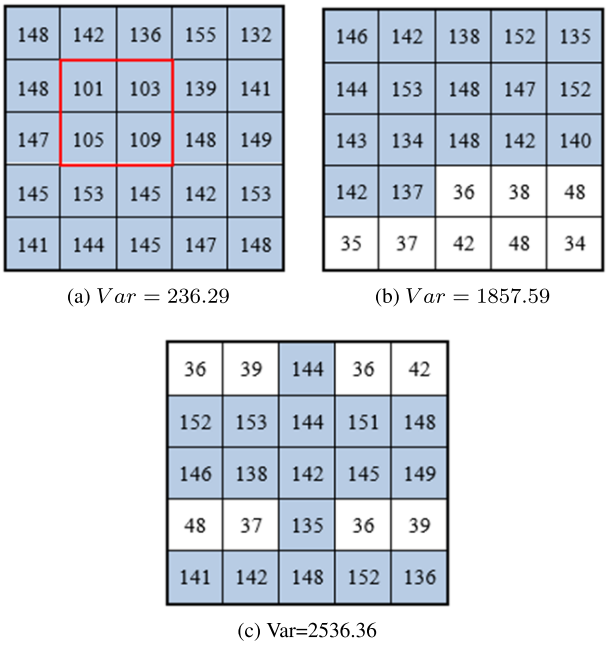

(a) $Var = 236.29$ (b) $Var = 1857.59$

(c) Var=2536.36

FIGURE 7. Different gray-scale distribution characteristics of infrared images of power equipment.

infrared imaging and the prerequisites of infrared sensors, infrared images usually have low resolution and blurred boundaries. In theory, the above problems can be effectively solved by IFCM.an decision-making process and is used to process data with uncertainty and ambiguity. At the same time, the intensity distribution of the infrared image is not uniform, which is caused by the uneven heat dissipation of the surface of the object, and the unevenness of the heat dissipation is reflected in the infrared image, which will bring difficulties to the segmentation, mainly leading to the lack of goals. As shown in Figure 6, the insulator portion is significantly darker than the isolation switch, so the FCM does not classify it as a target.

In response to the above problem, the method adopts the algorithm form of IFCM and combines the local intensity distribution information. The improved objective function is defined as follows:

$$J = u_{jk}^{m}[d_{IFS}^{2}(x_k, v_j) + \Omega \sum_{i \in n_k, i \neq k} \eta_{ik} d_{IFS}^{2}(x_i, v_j)] \quad (22)$$

$$\eta_{ik} = [(1 + Var(n_i))d_{ki}]^{-1}(1 - u_{ji})^{m} \quad (23)$$

where Ω controls the influence of local neighbor information, n_i denotes the neighborhood of x, η_{ik} measures the influence of x_i around x_k, $Var(n_i)$ is the variance of n_i, d_{ki} is the Euclidean spatial distance between x_i and x_k, and m is used as the blurring factor The value in this method is 2. $d_{IFS}(x_k, v_j)$ is defined in equation (11), and the fuzzification process of the infrared image actually increases the dimensionality of the data. The initial data has only one dimension, which is the gray value, but the converted data has three dimensions, including $u_A(x)$, $v_A(x)$ and $\pi_A(x)$. Hence, the cluster centroid is a three-dimensional vector, no longer the original intensity. The normalized Euclidean distance measure takes into account the degree of membership, non-affiliation and hesitation to measure the difference between the cluster centroid and the data points.

In the objective function, the variance of the local region and the spatial distance is used to control the influence of the intuitionistic blur distance between x_i and adjacent pixels. If the variance of the neighborhood is large, it means that there is a difference between the pixels in the area. Then adjacent pixels do not have much influence on determining the membership of x_i. As shown in equation (22), the value of η_{ik} will decrease as $Var(n_i)$ increases. Regional variance not only helps to maintain the details of the target, but also helps to resolve non-uniformity issues. As shown in Figure 7, (a) is a common form of uneven intensity distribution, the red area is part of the target, but the heat distribution is poor. Figure 7(b) shows the boundary structure between the target and the background. Figure 7 (c) shows the common structure of the insulator. It can be seen from the value of $Var(n_i)$ that the region variance of Fig. 7(a) is smaller than that of Figs. 7(b) and (c), which means that the pixel of Fig. 7(a) has greater similarity in the region. Therefore, adjacent pixels have a greater influence on the membership of the center point of Figure 7(a). Conversely, the independence between the center points of (b) and (c) and adjacent pixels is stronger. Hence, the center point of (a) is often classified into the same class as most of its neighbors. The boundary in (b) will not be mixed, and the tiny structure of the insulator in (c) will remain unchanged. At the same time, for a different x_i, when x_i is away from x_k, the weight will also decrease, because the similarity between pixels usually decreases with increasing distance. For class j, when the membership of adjacent pixels of x_k belonging to class j increases, the distance metric $\eta_{ik} d_{IFS}^{2}$ will become smaller, then x_k will tend to be classified as the jth class. As a result, pixels in the same area will have different degrees of homogeneity.

Figure 8 shows the difference between FCM, IFCM and the improved IFCM calculation results. In figure 8 (a), it can be seen that although the infrared image after FCM segmentation separates the cloud components in the sky, the wall cannot be separated from the electrical equipment due to

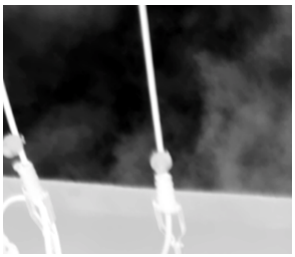

(a) Original image

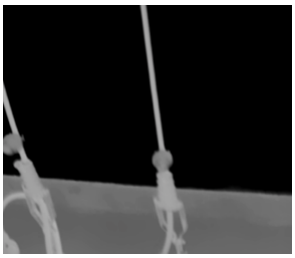

(b) FCM segmentation result diagram

(c) IFCM segmentation result diagram combining local information

FIGURE 8. Results of non-uniform image segmentation.

the similar strength of wire clip between the wall and the equipment, which is classified as the same target by FCM. Compared with FCM, the method proposed in this paper effectively improves the membership degree of nonhomogeneous regions. In addition, the influence of the neighborhood is also controlled within a range that fits the edges, boundaries and details. It can be seen from the results obtained by FCM that the divided power equipment is incomplete due to the lack of insulators, wires, etc. The segmentation results obtained from IFCM show more required power equipment targets than FCM, but still cant completely separate the device targets from the background. By improving the IFCM algorithm, the segmentation results make the power equipment more complete than the traditional IFCM, but also retain more details of the wire portion.

C. IMPROVED IFCM FORM BASED ON DISTRIBUTION INFORMATION

This paper summarizes the above improvements, and gives the objective function of the improved intuition FCM based on the distribution information, which can be expressed as follows:

$$J = \sum_{j=1}^{c}\sum_{k=1}^{n} W_{jk}u_{jk}^{m}[d_{IFS}^{2}(x_k, v_j) + \Omega \sum_{i\in n_k, i\neq k} \eta_{ik} d_{IFS}^{2}(x_i, v_j)] \quad (24)$$

where $\sum_{j=1}^{c} u_{jk} = 1, k = 1, 2, 3, \ldots, n$ and $\forall u_{jk} \in [0, 1]$. The specific expressions of W_{jk} and η_{ik} are as shown in the formula (19), the formula (20), and the formula (22). Using the Lagrange Multiplier method [41], the target function can be rewritten as follows:

$$F = \sum_{j=1}^{c}\sum_{k=1}^{n} W_{jk}(d_{IFS}^{2}(x_k, v_j) + \Omega \sum_{i\in n_k, i\neq k} \eta_{ik} d_{IFS}^{2}(x_i, v_j)) + \sum_{k=1}^{n} \lambda_k (\sum_{j=1}^{c} u_{jk} - 1) \quad (25)$$

1) CALCULATE U_{jk}

Since the value of η_{ik} depends on u_{jk}, the derivation method in [23] cannot be used when calculating the derivative for u_{jk}. And in the objective function of [29], there may be a case of missing parentheses, which leads to different problems. Hence, this paper uses the Lagrange Multiplier method to rewrite the objective function of the proposed algorithm to equation (25), where $\eta_{ik} = [(Var(n_k) + 1)d_{ki}]^{-1}(1 - u_{jk})^m$. Although the part of η_{ik} does not explicitly contain u_{jk}, u_{jk} belongs to the adjacent point x_{jk}. This means that u_{jk} will appear several times in $\sum_{j=1}^{c}\sum_{k=1}^{n} \Omega \sum_{i\in n_k, i\neq k} \eta_{ik} d_{IFS}^{2}(x_i, v_j)$ when calculating the first-order partial derivative of equation (24). The number of occurrences depends on the size and shape of the adjacent [42].

For example, in the algorithm proposed in this paper, the neighborhood is set to a square of size 3. In this case, is included in the neighborhood of its 8 neighbors. When calculating the derivative for, this article only retains the part containing, and rewrites equation (24) as follows:

$$f = W_{jk}u_{jk}^{m}[d_{IFS}^{2}(x_k, v_j) + \Omega \sum_{i\in n_k, i\neq k} \eta_{ik} d_{IFS}^{2}(x_i, v_j)] + \lambda_k (\sum_{j=1}^{c} u_{jk} - 1) + \Omega \sum_{i\in n_k, i\neq k} W_{ji}u_{ji}^{m}[(Var(n_i)+1)d_{ki}]^{-1} \times (1 - u_{jk})^m d_{IFS}^{2}(x_k, v_j) \quad (26)$$

Then the u_{jk} of the zero gradient condition is derived as follows:

$$\frac{\partial F}{\partial u_{jk}} = \frac{\partial f}{\partial u_{jk}} = mW_{jk}u_{jk}^{m-1}[d_{IFS}^{2}(x_k, v_j) + \Omega \sum_{i\in n_k, i\neq k} \eta_{ik} d_{IFS}^{2}(x_i, v_j)] + \lambda_k - m\Omega \sum_{i\in n_k, i\neq k} W_{ji}u_{ji}^{m}[(Var(n_i) + 1)d_{ki}]^{-1} \times (1 - u_{jk})^m d_{IFS}^{2}(x_k, v_j) = 0 \quad (27)$$

Set the blur factor m to 2. Equation (26) is as follows:

$$\frac{\partial F}{\partial u_{jk}} = 2W_{jk}u_{jk}^{m-1}[d_{IFS}^{2}(x_k, v_j) + \Omega \sum_{i\in n_k, i\neq k} \eta_{ik} d_{IFS}^{2}(x_i, v_j)] + \lambda_k$$

$$-2\Omega \sum_{i\in n_k, i\neq k} W_{ji}u_{ji}^m[(Var(n_i)+1)d_{ki}]^{-1} \times (1-u_{jk})^m d_{IFS}^2(x_k, v_j) = 0 \quad (28)$$

If this article makes $2W_{jk}u_{jk}^{m-1}(d_{IFS}^2(x_k, v_j) + \Omega \sum_{i\in n_k, i\neq k} \eta_{ik} d_{IFS}^2(x_i, v_j)) = A_{jk}$ and $2\Omega \sum_{i\in n_k, i\neq k} W_{ji}u_{ji}^m[(Var(n_i)+1)d_{ki}]^{-1}(1-u_{jk})^m d_{IFS}^2(x_k, v_j) = B$ at the same time, then there is:

$$A_{jk}u_{jk} + \lambda_k - B_{jk}(1-u_{jk}) = 0 \quad (29)$$

In conjunction with $\frac{\partial F}{\partial \lambda_k} = \sum_{j=1}^{c} u_{jk} - 1 = 0$, this paper can get the iterative recursive formula of u_{jk} as follows:

$$u_{jk} = (\frac{1}{A_{jk}+B_{jk}})(B_{jk} - \frac{\sum_{l=1}^{c} \frac{B_{lk}}{A_{lk}+B_{lk}} - 1}{\sum_{p=1}^{c} \frac{1}{A_{pk}+B_{pk}}}) \quad (30)$$

2) CALCULATE V_j AND λ_i

In order to minimize the objective function, the first-order partial derivatives of F on $v_j = [u(v_j), v(v_j), \pi(v_j)]$ and λ_i need to be calculated and set to 0. The first-order partial derivatives for v_j and λ_i are as follows:

$$\frac{\partial F}{\partial u(v_j)} = \sum_{k=1}^{n} W_{jk}u_{jk}(u(v_k) - u(v_j)) + \Omega \sum_{i\in n_k, i\neq k} \eta_{ik}(u(v_k) - u(v_j)) = 0 \quad (31)$$

$$\frac{\partial F}{\partial v(v_j)} = \sum_{k=1}^{n} W_{jk}u_{jk}(v(v_k) - v(v_j)) + \Omega \sum_{i\in n_k, i\neq k} \eta_{ik}(v(v_k) - v(v_j)) = 0 \quad (32)$$

$$\frac{\partial F}{\partial \pi(v_j)} = \sum_{k=1}^{n} W_{jk}u_{jk}(\pi(v_k) - \pi(v_j)) + \Omega \sum_{i\in n_k, i\neq k} \eta_{ik}(\pi(v_k) - \pi(v_j)) = 0 \quad (33)$$

$$\frac{\partial F}{\partial \lambda_k} = \sum_{k=1}^{n} u_{jk} - 1 = 0 \quad (34)$$

Further, this paper can get the iterative formula derived from $v_j = [u(v_j), v(v_j), \pi(v_j)]$:

$$u(v_j) = \frac{\sum_{k=1}^{n} W_{jk}u_{jk}^m[u(x_k) + \Omega \sum_{i\in n_k, i\neq k} \eta_{ik}u(x_i)]}{\sum_{k=1}^{n} W_{jk}u_{jk}^m(\Omega \sum_{i\in n_k, i\neq k} \eta_{ik} + 1)} \quad (35)$$

$$v(v_j) = \frac{\sum_{k=1}^{n} W_{jk}u_{jk}^m[v(x_k) + \Omega \sum_{i\in n_k, i\neq k} \eta_{ik}v(x_i)]}{\sum_{k=1}^{n} W_{jk}u_{jk}^m(\Omega \sum_{i\in n_k, i\neq k} \eta_{ik} + 1)} \quad (36)$$

$$\pi(v_j) = \frac{\sum_{k=1}^{n} W_{jk}u_{jk}^m[\pi(x_k) + \Omega \sum_{i\in n_k, i\neq k} \eta_{ik}\pi(x_i)]}{\sum_{k=1}^{n} W_{jk}u_{jk}^m(\Omega \sum_{i\in n_k, i\neq k} \eta_{ik} + 1)} \quad (37)$$

3) ALL CALCULATION STEPS

The algorithm calculation process proposed in this paper is as follows:

Step 1, use the equations (8)-(10) to visually obfuscate the original image data.

Step 2, initialize parameters c, m and membership matrix U.

Step 3, update cluster centroid v_j and membership degree u_jk according to equation (29) and equations (34)-(36).

Step 4, check if a is satisfied; if not, return to the previous step.

4) PARAMETERS ANALYSIS

In the following, numerical analysis is performed on Ω, λ and γ involved in the data fuzzification process. The parameter Ω is used as the weight of the local distribution information to control the influence of the local information of the image, the parameter λ is used as the intuitionistic fuzzy supplementary parameter and is proportional to the degree of hesitation of a point, and the parameter γ is used as the center distance difference weight to control the distance between the data point and the target center In a valid range, this makes the membership of the data points in the target area mainly determined by the intensity rather than the spatial information. In order to judge the performance of the algorithm under different parameters, two quantitative indicators of relative foreground area error (RAE) and error score (ME) are used. (RAE reflects the difference between the target segmentation image and the reference segmentation image in the shape and shape of the target, and reflects the accuracy of the target feature extraction; ME reflects the ratio of the background of the segmented image into the foreground, which is an important indicator of staggered pixels). The range of quantified evaluation indexes for both image segmentation is [0, 1]. The smaller the value, the better the segmentation effect on the target image.

Experiment with the original gray image composition data set above: set the parameter range to [0, 4] with a step size of 0.5. Figure 9 is obtained after experimental and numerical analysis of the image in this paper. From Figure 9 (a), it can be confirmed that the ME curve tends to stabilize after the value of Ω exceeds 1.5, while the RAE curve starts to slowly rise after 2.5 Generally speaking, compared to ME, RAE is more sensitive to changes in segmentation targets and has a closer relationship with the quality of visual effects. Therefore, it is determined to be 2.5 after considering the change trend of the two curves. Similarly, set the range of the parameter λ to [1, 6] with a step size of 0.5. In Figure 9 (b), it can be clearly observed that the ME and RAE values both reach the minimum value at 1.2, so λ is determined to be 1.2; set the

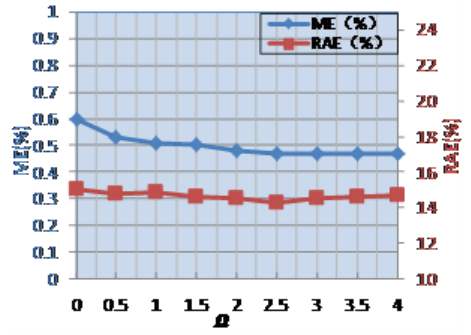

(a)

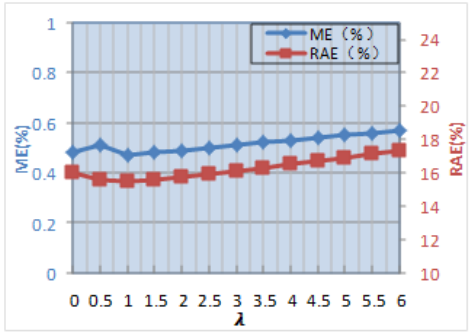

(b)

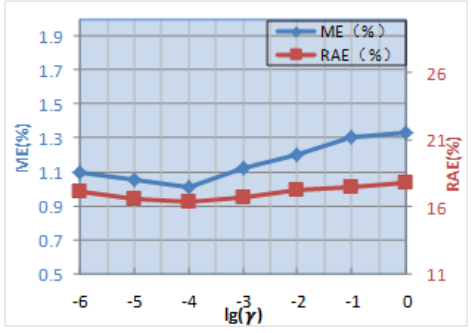

(c)

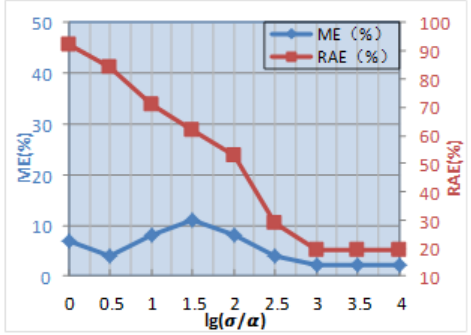

(d)

FIGURE 9. Line chart of ME and RAE with different values of parameters Ω, λ, $lg(\lambda)$, $lg(\sigma/\alpha)$.

value range of parameter γ to $[10^{-6}, 1]$, that is, the value range of $lg(\lambda)$ is $[-6, 0]$, and the step size is 1. It is observed from Figure 9 (c) that the ME and RAE values both reach the minimum value at $lg(\gamma) = -4$, so it is determined $\gamma = 10^{-4}$.

For the two parameters and that will change ME and RAE as the ratio changes, finding the relationship between the two through experiments. Try to set the value range of σ/α to $[1, 10^4]$, that is, the value range of $lg(\sigma/\alpha)$ is $[0, 4]$. It is observed from Figure 9 (d) that the segmentation effect is best when $lg(\sigma/\alpha)$ is in the interval of $(3, 4)$. After trying different values of α and σ, set α to 8, and σ to 3. At this time, the fixed value β obtained from $\beta = 1/\sqrt{2\pi\sigma}$ is 0.1.

In summary, it can be seen from Figure 9 that the parameter curve remains stable and presents a smooth shape, indicating that the algorithm in this paper can maintain a high level and is not sensitive to parameters in a specific range. The parameter settings of the algorithm are shown in Table 1.

TABLE 1. Units for Magnetic Properties.

Symbol	Specific meaning	Value
m	Furzzy factor	2
β	Fixed value of possible area	0.1
λ	Intuitionistic fuzzy supplementary parameter	1.2
σ/α	Center distance weight	4000
γ	Center distance difference weight	10^{-4}
Ω	Local distributed information weight	2.5

D. SEGMENTATION PERFORMANCE TESTING AND ANALYSIS

In order to verify the performance of the algorithm, the proposed method is compared with the six widely used segmentation methods of FCM, FLICM, KIFCM, GQFCM, IFCM and PIFCM. The data set used is 300 images of different types and backgrounds of power equipment obtained by the laboratory using the FLIR E75 thermal imager. The types of power equipment included are insulators, equipment clips, isolating switches, wall bushings, etc., and there are complex backgrounds in the image, such as man-made buildings, vegetation, cloud weather and commuter vehicles. Each image in the dataset is 320*240 pixels in size. This paper assumes that the infrared image used in the experiment contains both the power device and the background, so the number of clusters of the algorithm is 2. For other clustering-based methods such as FCM, FLICM, IFCM, GQFCM, etc., through a series of tests, the number of clusters is set to 3, and the cluster with the highest intensity is set as power equipment. For other cluster-based methods such as FCM, FLICM, FCM, GQ FCM, through a series of tests, setting the number of clusters to 3, and setting the cluster with the highest intensity as power equipment. A good result was obtained when the index of the generation function in IFCM and PIFCM was set to 0.9. In particular, this article uses the same parameter settings as [31] for KIFCM.

The data set tested in this paper contains several typical scenarios involving three main problems in infrared segmentation of power equipment, including low-contrast scenes, high-intensity non-target object interventions, and non-uniform intensity targets.

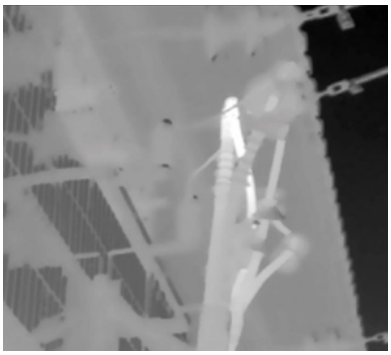

(a) A typical scene with low contrast

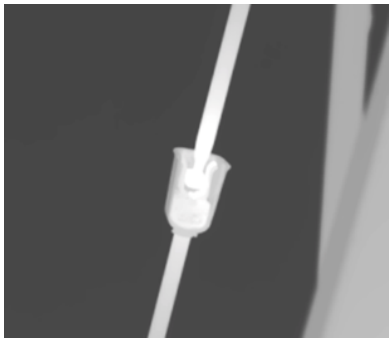

(b) Typical scenes containing high intensity non-target objects

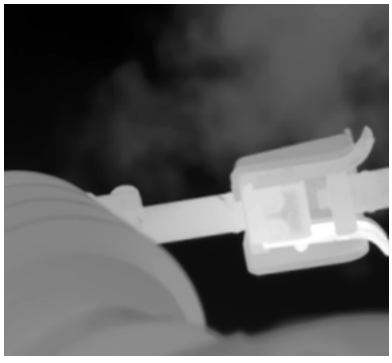

(c) Typical scenarios with uneven intensity targets

FIGURE 10. Three typical scenarios.

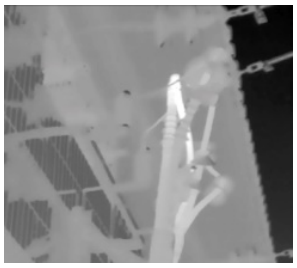

(a) Original image

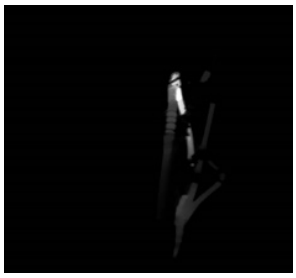

(b) algorithm in this paper

(c) FCM

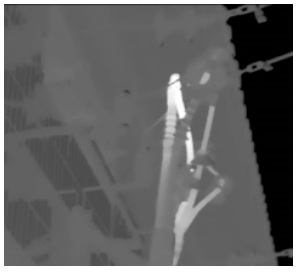

(d) KIFCM

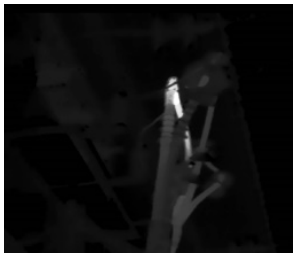

(e) GQFCM

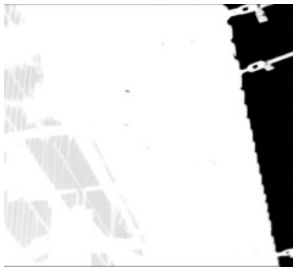

(f) FLICM

(g) PIFCM

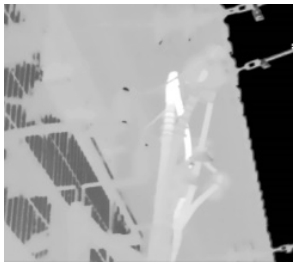

(h) IFCM

FIGURE 11. Segmentation results of various algorithms.

In this case, the power equipment will partially blend into the background, as shown in Figure 10(a). The ambiguity of the outline of the power equipment makes it difficult to accurately segment. Especially for the cluster-based algorithm, since the center positions of different clusters are very close, the segmentation result is easy to present a state of almost white or all black.

There are usually other high-intensity targets in the infrared image of power equipment, as shown in Figure 10(b). Although these targets are usually located in the edge region and have different shape or structural information than the real target, many segmentation methods are difficult to ignore their interference, which is mainly because the intensity information is the dominant factor of these methods.

Due to the different physical properties of the heat dissipation amount, the power equipment inevitably exhibits a state in which the intensity distribution is uneven in thermal imaging. This feature often leads to fragmentation results and severely affects the quality of the segmentation, as shown in Figure 10(c).

Figure 11-13 shows the segmentation results for some typical scenarios summarized in Figure 10 above. The infrared image with a large number of artificial architectural backgrounds in Figure 11 has obvious low contrast characteristics, which is the difficulty of segmentation. As shown, the outline of the wall bushing is almost mixed with the background. For cluster-based methods such as FCM, FLICM, IFCM, and KIFCM, the existing cluster information is very close due to

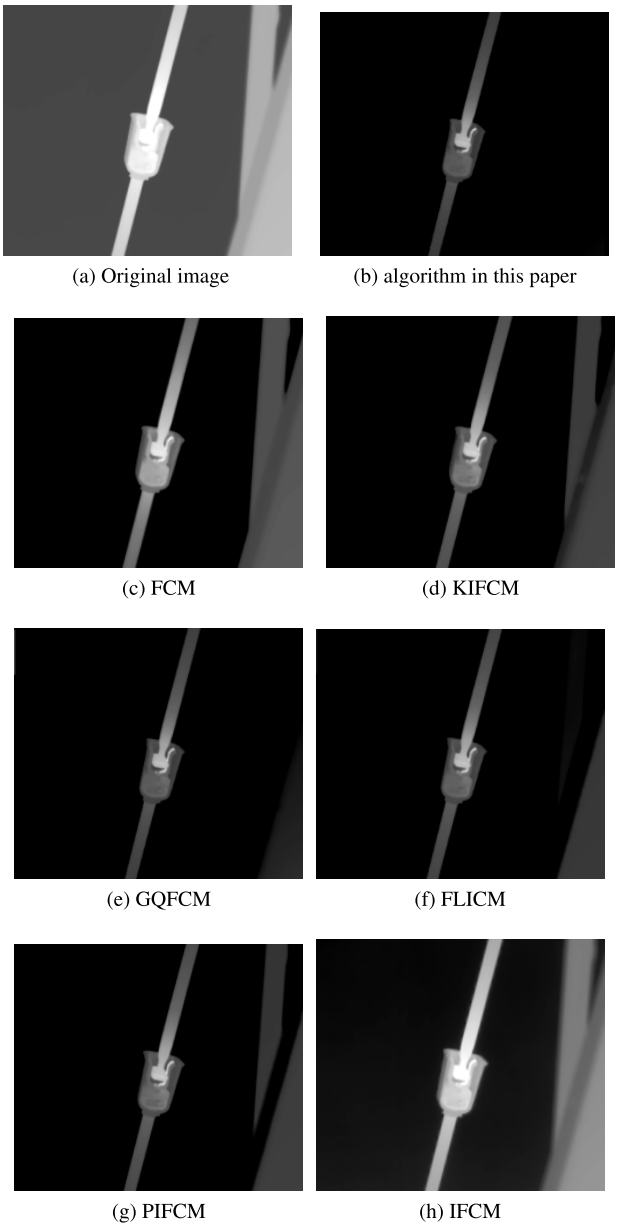

(a) Original image (b) algorithm in this paper

(c) FCM (d) KIFCM

(e) GQFCM (f) FLICM

(g) PIFCM (h) IFCM

FIGURE 12. Segmentation results of various algorithms.

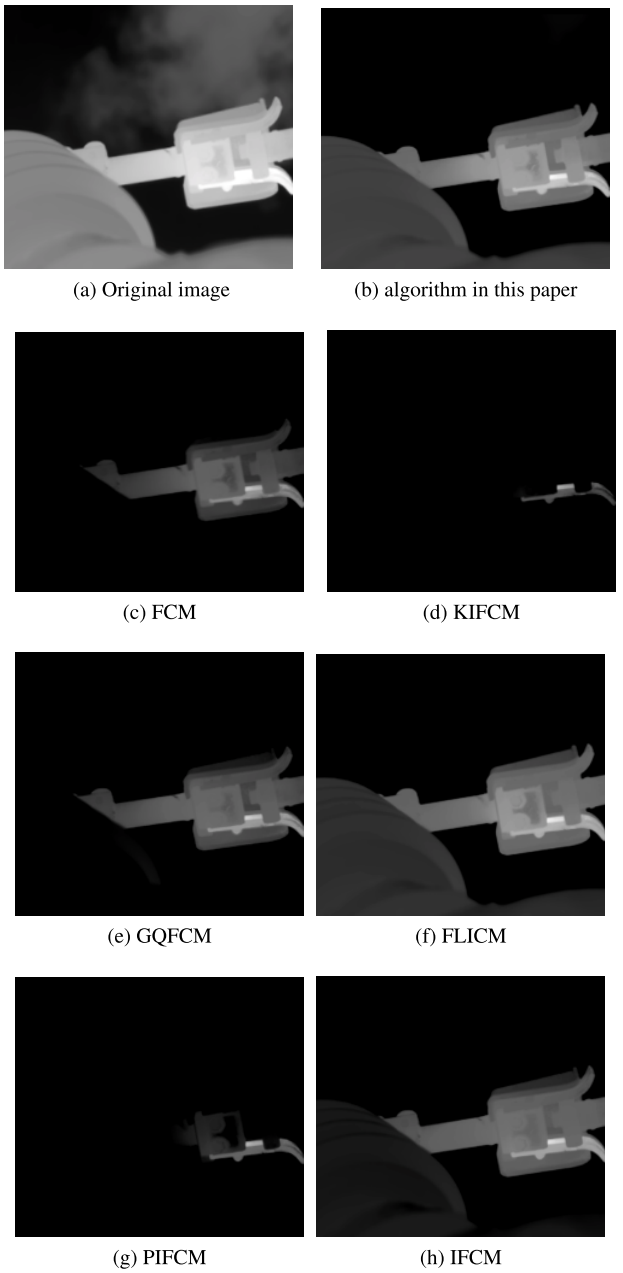

(a) Original image (b) algorithm in this paper

(c) FCM (d) KIFCM

(e) GQFCM (f) FLICM

(g) PIFCM (h) IFCM

FIGURE 13. Segmentation results of various algorithms.

insufficient spatial information, and the background of the segmented image still exists. GQFCM can only split a small portion of a wall bushing on a relatively clear boundary, but the PIFCM method and the proposed method get close to real results. However, if the PIFCM is compared with the results of the proposed method and the real image, this paper will find that the edge part of the target has different degrees of loss in the PIFCM results. Compared to other methods, this method suppresses noise and clutter interference and preserves more edge detail in low contrast situations.

Figure 12 is a scene of a non-powered equipment containing high intensity, surface reflections. Since FCM and KIFCM do not contain spatial information, the results are greatly affected by surface reflection. The calculation results of IFCM method, PIFCM method and FLICM method all contain relatively complete equipment. However, they cannot completely distinguish between equipment and non-equipment. GQFCM and the proposed method can effectively eliminate the interference of non-power equipment and reflection, and get a more realistic result. But the results of GQFCM still contain a small portion of the non-equipment of the image. In general, this method is stable in low contrast conditions and can handle high-intensity non-target objects well. It has also been found that this method can effectively improve the non-uniformity and reflection problems.

As shown in Figure 13, there is significant intensity non-uniformity in the main body of the power equipment. Due to the lack of local spatial information, several methods

TABLE 2. Average time used by each algorithm (unit: milliseconds).

Algorithm	Average Time
Proposed	1708.9
FCM	1678.2
KIFCM	2578.3
GQFCM	438.1
FLICM	12861.4
PIFCM	7257.2
IFCM	653.6

based on fuzzy clustering are not satisfactory. The results of the FLICM method are more complete, but a portion of the insulator is lost, which can have a significant impact on subsequent processing operations. The results show that the method effectively suppresses the target non-uniformity while retaining the target details.

It can be seen that FCM and KIFCM perform similarly in the above scenarios, and the kernel function used in KIFCM has a limited effect on suppressing the background. However, the use of local spatial information in FLICM and IFCM improves the effect of uneven intensity to some extent, but still cannot effectively deal with the effects of low contrast. PIFCM uses adaptive weighted intuitionistic fuzzy distance measurement, which works well in low contrast and anti-reflection, but non-target objects cannot be removed by PIFCM. GQFCM combines the Markov random field with shape information and uses the geometric mean of the two reusable energy levels represented by the Gibbs random field distribution to polarize the membership values on the boundary. It performs well in suppressing the light background and intensity inhomogeneity. If the image contains part of the light background, the spatial information involved is too weak to suppress the background. However, in the method of this paper, the use of global distribution information helps to suppress backgrounds containing high-intensity non-targets. When the target is affected by intensity inhomogeneity, reflectivity and clutter, the intuitionistic blur distance combined with the local distribution information can also give more complete results.

In order to compare the segmentation efficiency of this algorithm, it is compared with other six segmentation algorithms in time. As shown in Table 1, the algorithm in this paper is improved based on IFCM and injected with local spatial information, so its efficiency is not as good as IFCM, among which the segmentation algorithm is not the highest, but compared to the image segmentation effect, it is still an excellent one among these seven algorithms.

For the effectiveness of the proposed method, this paper uses the relative foreground region error (RAE) to comprehensively judge the quality of segmentation results of the above segmentation algorithms.

RAE reflects the accuracy of target segmentation. In the application of image analysis of power equipment in this paper, it mainly focuses on the foreground rather than the whole image, which makes it sensitive to power equipment.

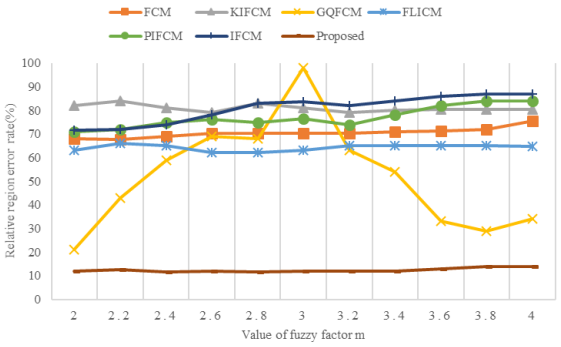

FIGURE 14. Relative regional error rate of fuzzy clustering algorithm measured under different m values.

TABLE 3. Relative area error rate data distribution of the measured fuzzy clustering algorithm under different m values (%)).

Value of m	FCM	KIFCM	GQFCM	FLICM	PIFCM	IFCM	Proposed
2.0	68.1	82.1	21.1	63.0	71.2	71.5	12.1
2.2	67.8	84.2	43.2	66.2	72.3	72.3	12.5
2.4	68.9	81.2	58.9	65.1	74.8	74.1	11.8
2.6	70.2	78.9	68.8	61.8	76.2	77.9	12.1
2.8	70.2	83.1	68.2	61.9	75.4	83.2	11.8
3.0	70.2	81.2	97.8	62.8	76.5	83.5	12.1
3.2	70.2	79.3	63.4	65.1	74.3	82.4	11.9
3.4	71.1	80.2	54.2	65.2	78.1	84.1	12.3
3.6	71.4	80.5	33.1	65.1	81.8	85.9	13.2
3.8	71.9	80.4	28.8	65.2	84.3	86.8	14.2
4.0	75.5	80.5	33.6	64.8	84.2	86.9	14.2

The expression of RAE is as follows:

$$RAE = \begin{cases} (F_T - F_S)/F_T & F_T > F_S \\ (F_S - F_T)/F_S & F_T < F_S \end{cases} \tag{38}$$

It can be seen from the above formula that in practical applications, the lower the RAE value, the better the segmentation effect. The RAE for testing various segmentation algorithms is shown in Figure 14 and Table 3. It can be seen from the line graph that the method in this paper maintains relative stability within the range of the fuzzy factor m relative to other algorithms, and obtains the optimal RAE value. The results show that the proposed method in this paper is robust and effective for the variation of the fuzzy factor m.

IV. CONCLUSION

With the rapid development of remote sensing in the field of UAVs, the efficiency and real-time monitoring of infrared UAVs for power equipment has attracted more and more attention and research. After the infrared drone captures the data of the power equipment, the diagnosis of the thermal fault of the power equipment will be an important research direction. In this paper, an infrared image segmentation IFCM algorithm for power equipment with spatial distribution information is proposed. Due to the low contrast between the power equipment and the background, and the interference of non-power equipment such as high-intensity artificial buildings, commuter vehicles and clouds, it usually has a serious

impact on equipment segmentation. At the same time, uneven surface heat dissipation can also cause uneven distribution of gray values of infrared images, which causes missing partial target contours after segmentation. Aiming at the above problems, a fuzzy clustering algorithm for introducing global spatial distribution information of Gaussian model is designed. The algorithm adopts a new ranging method, which changes the membership degree of each pixel with the change of distance, effectively suppresses the high-intensity background, and highlights the effective target in the segmentation result. On this basis, the local intensity distribution information composed of intuitionistic fuzzy c-means composed of local variance and neighborhood membership is combined. Using intuitionistic fuzzy distance and local distribution information to solve the problem of uneven intensity. The segmentation effect of the algorithm and other similar algorithms was tested on a power equipment dataset containing 300 images. After comparing the visual effects and quantitative comparison of the results, the method is superior to FCM, KIFCM, GQFCM, FLICM, PIFCM, IFCM and other algorithms in terms of effective target detail retention and accuracy after segmentation of the same image and the segmentation of the infrared image of the device is effective.

REFERENCES

[1] L. Zhu-Mao, L. Qing, J. Tao, L. Yong-Xin, H. Yu, and B. Yang, "Research on thermal fault detection technology of power equipment based on infrared image analysis," in *Proc. IEEE 3rd Adv. Inf. Technol., Electron. Autom. Control Conf. (IAEAC)*, Oct. 2018, pp. 2567–2571.

[2] X. Perpina, F. Reverter, J. Leon, E. Barajas, M. Vellvehi, X. Jorda, and J. Altet, "Output power and gain monitoring in RF CMOS class a power amplifiers by thermal imaging," *IEEE Trans. Instrum. Meas.*, vol. 68, no. 8, pp. 2861–2870, Aug. 2019.

[3] P. F. Xu, J. Zhang, T. F. Yin, X. X. Qian, and Y. Yang, "Research on image segmentation of power equipment based on improved PCNN algorithm," *Intell. Comput. Appl.*, vol. 9, no. 3, pp. 59–62 and 68, 2019.

[4] C. B. Yu, L. Zeng, and L. Zhang, "Multi-point fault segmentation of electrical equipment based on OTSU and regional growth," *Infr. Technol.*, vol. 40, no. 10, pp. 1008–1012, 2008.

[5] Z. J. Wang, S. F. Niu, X. X. Liu, and R. H. Cui, "Study on application of bat algorithm to optimize two-dimensional entropy for infrared image segmentation of transformer equipment," *Electron. Des. Eng.*, vol. 26, no. 18, pp. 83–87, 2008.

[6] X. Li, H. Y. Cui, S. J. Huo, J. Shu, C. F. Liu, Y. Li, and G. F. Li, "Infrared image segmentation of Niblack power equipment based on particle swarm optimization," *Infr. Technol.*, vol. 40, no. 8, pp. 780–785, 2014.

[7] S. Kapil, M. Chawla, and M. D. Ansari, "On K-means data clustering algorithm with genetic algorithm," in *Proc. 4th Int. Conf. Parallel, Distrib. Grid Comput. (PDGC)*, 2016, pp. 202–206.

[8] K. T. Atanassov, "Intuitionistic fuzzy sets," *Fuzzy Sets Syst.*, vol. 20, no. 1, pp. 87–96, Aug. 1986, doi: 10.1016/S0165-0114(86)80034-3.

[9] N. Pelekis, D. K. Iakovidis, E. E. Kotsifakos, and I. Kopanakis, "Fuzzy clustering of intuitionistic fuzzy data," *Int. J. Bus. Intell. Data Mining*, vol. 3, no. 1, pp. 45–65, 2008.

[10] Z. Xu and J. Wu, "Intuitionistic fuzzy C-means," *J. Syst. Eng. Electron.*, vol. 21, no. 4, pp. 580–590, 2010.

[11] K.-P. Lin, "A novel evolutionary kernel intuitionistic fuzzy *C*-means clustering algorithm," *IEEE Trans. Fuzzy Syst.*, vol. 22, no. 5, pp. 1074–1087, Oct. 2014.

[12] Q. M. D. Lohani, R. Solanki, and P. K. Muhuri, "Novel adaptive clustering algorithms based on a probabilistic similarity measure over Atanassov intuitionistic fuzzy set," *IEEE Trans. Fuzzy Syst.*, vol. 26, no. 6, pp. 3715–3729, Dec. 2018.

[13] F. Zhao, Y. Chen, H. Liu, and J. Fan, "Alternate PSO-based adaptive interval type-2 intuitionistic fuzzy C-means clustering algorithm for color image segmentation," *IEEE Access*, vol. 7, pp. 64028–64039, 2019.

[14] C. L. Chowdhary and D. P. Acharjya, "A hybrid scheme for breast cancer detection using intuitionistic fuzzy rough set technique," *Int. J. Healthcare Inf. Syst. Inform.*, vol. 11, no. 2, pp. 38–61, Apr. 2016, doi: 10.4018/978-1-5225-0983-7.ch047.

[15] C. V. Negoita, "Fuzzy sets," *Fuzzy Sets Syst.*, vol. 133, no. 2, p. 275, Jan. 2003, doi: 10.1016/s0165-0114(02)00361-5.

[16] F. Gomide, "Uncertain rule-based fuzzy logic systems: Introduction and new directions," *Fuzzy Sets Syst.*, vol. 133, no. 1, pp. 133–135, Jan. 2003, doi: 10.1016/s0165-0114(02)00359-7.

[17] J. Mendel, "Computing derivatives in interval type-2 fuzzy logic systems," *IEEE Trans. Fuzzy Syst.*, vol. 12, no. 1, pp. 84–98, Feb. 2004, doi: 10.1109/tfuzz.2003.822681.

[18] J. C. Dunn, "A fuzzy relative of the ISODATA process and its use in detecting compact well-separated clusters," *J. Cybern.*, vol. 3, no. 3, pp. 32–57, Jan. 1973.

[19] J. C. Bezdek, "Fuzzy mathematics in pattern classification," Ph.D. dissertation, Cornell Univ., New York, NY, USA, 1973.

[20] M. Sugeno, "Fuzzy measures and fuzzy integrals—A survey," *Readings Fuzzy Sets Intell. Syst.*, vol. 6, no. 1, pp. 251–257, 1993.

[21] W. Wang and X. Xin, "Distance measure between intuitionistic fuzzy sets," *Pattern Recognit. Lett.*, vol. 26, no. 13, pp. 2063–2069, Oct. 2005.

[22] E. Szmidt and J. Kacprzyk, "Distances between intuitionistic fuzzy sets," *Fuzzy Sets Syst.*, vol. 114, no. 3, pp. 505–518, Sep. 2000.

[23] R. Solanki, Q. M. D. Lohani, and P. K. Muhuri, "A novel clustering algorithm based on a new similarity measure over Intuitionistic fuzzy sets," in *Proc. IEEE Int. Conf. Fuzzy Syst. (FUZZ-IEEE)*, Aug. 2015, pp. 1–8.

[24] I. Vlachos and G. Sergiadis, "Towards intuitionistic fuzzy image processing," in *Proc. Int. Conf. Comput. Intell. Modelling, Control Automat. Int. Conf. Intell. Agents, Web Technol. Internet Commerce (CIMCA-IAWTIC)*, May 2006, pp. 2–7.

[25] Q. D. Lohani, R. Solanki, and P. K. Muhuri, "A convergence theorem and an experimental study of intuitionistic fuzzy c-mean algorithm over machine learning dataset," *Appl. Soft Comput.*, vol. 71, pp. 1176–1188, Oct. 2018.

[26] G. A. W. West and T. A. Clarke, "A survey and examination of subpixel measurement techniques," *Proc. SPIE*, vol. 1395, no. 3, pp. 456–462, 1990.

[27] X. Bai, Z. Chen, Y. Zhang, Z. Liu, and Y. Lu, "Infrared ship target segmentation based on spatial information improved FCM," *IEEE Trans. Cybern.*, vol. 46, no. 12, pp. 3259–3271, Dec. 2016.

[28] T. Chaira, "A novel intuitionistic fuzzy C means clustering algorithm and its application to medical images," *Appl. Soft Comput.*, vol. 11, no. 2, pp. 1711–1717, Mar. 2011.

[29] T. Chan and L. Vese, "Active contours without edges," *IEEE Trans. Image Process.*, vol. 10, no. 2, pp. 266–277, Feb. 2001.

[30] Z. Liu, F. Zhou, X. Chen, X. Bai, and C. Sun, "Iterative infrared ship target segmentation based on multiple features," *Pattern Recognit.*, vol. 47, no. 9, pp. 2839–2852, Sep. 2014.

[31] X. Bai, Y. Wang, H. Liu, and S. Guo, "Symmetry information based fuzzy clustering for infrared pedestrian segmentation," *IEEE Trans. Fuzzy Syst.*, vol. 26, no. 4, pp. 1946–1959, Aug. 2018.

[32] Z. Fan, C. Wang, and X. Ma, "Double-threshold image segmentation method based on gray gradient," *Proc SPIE*, vol. 7506, Dec. 2009, Art. no. 75062O.

[33] S. Shyrai and D. A. Viattchenin, "Clustering the intuitionistic fuzzy data: Detection of an unknown number of intuitionistic fuzzy clusters in the allotment," in *Proc. Int. Conf. Inf. Digit. Technol.*, Zilina, Slovakia, Jul. 2015, pp. 314–323.

[34] H. Jiang, X. Zhou, B. Feng, and M. Zhang, "A new intuitionistic fuzzy c-means clustering algorithm," in *Proc. Int. Conf. Mechatronic Sci., Electr. Eng. Comput. (MEC)*, Shengyang, China, Dec. 2013, pp. 1116–1119.

[35] Y. Du, G. Wu, and G. Tang, "Auto-encoder based clustering algorithms for intuitionistic fuzzy sets," in *Proc. 12th Int. Conf. Intell. Syst. Knowl. Eng. (ISKE)*, Nanjing, China, Nov. 2017, pp. 1–6.

[36] R.-X. Ding, X. Wang, K. Shang, B. Liu, and F. Herrera, "Sparse representation-based intuitionistic fuzzy clustering approach to find the group intra-relations and group leaders for large-scale decision making," *IEEE Trans. Fuzzy Syst.*, vol. 27, no. 3, pp. 559–573, Mar. 2019.

[37] Z. Xi-Yang, W. Xiao-Li, and L. Liang-Qun, "Online multi-object tracking via maximum entropy intuitionistic fuzzy data association," in *Proc. 14th IEEE Int. Conf. Signal Process. (ICSP)*, Beijing, China, Aug. 2018, pp. 803–806.

[38] M. Kaushal, R. Solanki, Q. D. Lohani, and P. K. Muhuri, "A novel intuitionistic fuzzy set generator with application to clustering," in *Proc. IEEE Int. Conf. Fuzzy Syst. (FUZZ-IEEE)*, Rio de Janeiro, Brazil, Jul. 2018 pp. 1–8.
[39] Y. Wang, Y. Lei, Y. Lei, and X. Fan, "Multi-factor high-order intuitionistic fuzzy time series forecasting model," *J. Seismol. Earthq. Eng.*, vol. 27, no. 5, pp. 1054–1062, Oct. 2016.
[40] Y. Yin and S. Xian, "Multi-criteria intuitionistic fuzzy decision making method with unknown weights based on experts classification," in *Proc. 2nd Int. Conf. Artif. Intell. Big Data (ICAIBD)*, Chengdu, China, May 2019, pp. 229–237.
[41] K.-P. Lin, K.-C. Hung, and C.-L. Lin, "Rule generation based on novel kernel intuitionistic fuzzy rough set model," *IEEE Access*, vol. 6, pp. 11953–11958, 2018.
[42] M. M. Dewi and H. Al Fatta, "Supplier selection using combined method of K-means and intuitionistic fuzzy topsis," in *Proc. Int. Seminar Appl. Technol. Inf. Commun.*, Semarang, Indonesia, Sep. 2018, pp. 394–399.

FANKUI HU was born in Jining, Shandong, China, in 1996. He received the B.S. degree in electronic information science and technology from Heilongjiang University, in 2018, where he is currently pursuing the master's degree. His main research direction is remote sensing image processing.

HAIBING CHEN was born in Nantong, Jiangsu, China, in 1995. He received the B.S. degree in electronics and information engineering from the Shanghai University of Electric Power, in 2017. He is currently pursuing the master's degree with Heilongjiang University. His main research direction is remote sensing image processing.

XIAOFEI WANG was born in Harbin, Heilongjiang, China, in 1977. He received the B.S. degree in environmental science and engineer from Nankai University, Tianjin, China, in 2001, and the M.S. and Ph.D. degrees in signal and information processing from the Harbin Institute of Technology (HIT), Harbin, China, in 2005 and 2011, respectively. He is currently an Associate Professor with the College of Electronics and Engineering, Heilongjiang University. His research interests include hyperspectral data analysis and image processing, multisource information fusion, pattern recognition, and classification.